

Circumbinary planets II - when transits come and go

David. V. Martin[★]

Observatoire de Genève, Université de Genève, 51 chemin des Maillettes, Sauverny 1290, Switzerland

Accepted . Received

ABSTRACT

Circumbinary planets are generally more likely to transit than equivalent single-star planets, but practically the geometry and orbital dynamics of circumbinary planets make the chance of observing a transit inherently time-dependent. In this follow-up paper to [Martin & Triaud \(2015\)](#), the time-dependence is probed deeper by analytically calculating when and for how long the binary and planet orbits overlap, allowing for transits to occur. The derived equations are applied to the known transiting circumbinary planets found by *Kepler* to predict when future transits will occur, and whether they will be observable by upcoming space telescopes *TESS*, *CHEOPS* and *PLATO*. The majority of these planets spend less than 50% of their time in a transiting configuration, some less than 20%. From this it is calculated that the known *Kepler* eclipsing binaries likely host an additional $\sim 17 - 30$ circumbinary planets that are similar to the ten published discoveries, and they will ultimately transit some day, potentially during the *TESS* and *PLATO* surveys.

Key words: binaries: close, eclipsing – astrometry and celestial mechanics: celestial mechanics, eclipses – planets and satellites: detection, dynamical evolution and stability, fundamental parameters – methods: analytical

1 INTRODUCTION

As early as the 1930's, people marvelled at the then science fiction concept of a planet orbiting two stars - a circumbinary planet ([Rudaux 1937](#)). Astronomers have contemplated their existence and characteristics even before the birth of exoplanet discoveries. [Borucki & Summers \(1984\)](#) noted that photometric searches around eclipsing binaries would have enhanced transit probabilities, which was later expanded upon by [Schneider & Chevreton \(1990\)](#) and [Schneider \(1994\)](#). After the unambiguous discovery of the first transiting circumbinary planet *Kepler-16* ([Doyle et al. 2011](#)) the field has flourished, leading to an additional ten transiting discoveries (the latest being *Kepler-1647* by [Kostov et al. 2016](#)) and a wealth of related studies.

For a circumbinary planet to transit it must pass in front of a moving target. This is fundamentally different to a stationary single star, and leads to enhanced transit timing variations ([Agol et al. 2005](#); [Holman & Murray 2005](#); [Armstrong et al. 2013](#)) and transit duration variations ([Kostov et al. 2014](#); [Liu et al. 2014](#)). If the planet and binary orbits are coplanar then transits are only possible on eclipsing binaries, but in this case transits are guaranteed once per planet orbit. If the planet and binary orbits are misaligned then transits are still possible, even on non-eclipsing binaries, but there will be gaps in the transit sequence and asymmetries in the

transit profiles ([Martin & Triaud 2014](#)). The picture is further complicated by the rapid orbital dynamics of circumbinary systems, caused by perturbations from the binary. The planet's orbit precesses on an observationally-relevant timescale of years ([Schneider 1994](#); [Farago & Laskar 2010](#); [Doolin & Blundell 2011](#); [Leung & Hoi Lee 2013](#)). Consequently, the state of the planet and binary orbits overlapping on the sky - essential for transits - changes with time, as was seen in the discovery of *Kepler-413* ([Kostov et al. 2014](#)).

Knowing the probability and time-dependence of circumbinary transits has wide implications, including:

- De-biasing observations to infer properties about circumbinary architectures and abundance ([Armstrong et al. 2014](#); [Martin & Triaud 2014](#); [Li et al. 2016](#)).
- Scheduling future photometric observations, both of known-transiting systems and ones found by alternative methods, e.g. eclipse timing variations ([Schwarz et al. 2011, 2016](#)), radial velocities ([Konacki et al. 2009](#)) and astrometry ([Sahlmann et al. 2014](#)).
- Predicting discovery yields for transit surveys, like *Kepler* in years gone by ([Martin & Triaud 2014](#)) and *TESS* and *PLATO* to come ([Li et al. 2016](#)).
- Understanding the fundamental differences between single and binary star systems, and in some cases exploiting the advantageous properties of circumbinary planets ([Borucki & Summers 1984](#); [Schneider 1994](#); [Martin & Triaud 2014, 2015](#); [Li et al. 2016](#)).

[★] E-mail: david.martin@unige.ch

much more efficient than using N-body integrations, and also better illuminates the geometry and orbital dynamics. However, unlike for single stars, it is not trivial to make such calculations for circumbinary planets. To help the analysis, in [Martin & Triaud \(2014\)](#) we formally defined the concept of *transitability*: a state in which the planet and binary orbits overlap on the sky, meaning that transits are possible but not guaranteed on every passing of the binary orbit. Transit probabilities were calculated numerically using N-body simulations for a handful of example systems, mainly applicable to the *Kepler* mission, and shown to be generally higher than for equivalent single-star planets. The next goal has been to calculate *analytically* the circumbinary transit probability, for any configuration and over any observing timespan. This task has been split into a series of three papers, of which this present paper constitutes the juicy meat in the circumbinary sandwich:

(i) [Martin & Triaud \(2015\)](#): analytic derivation of the probability that a given circumbinary planet would enter transitability at some *unspecified* point in time. It was shown numerically that transitability ultimately guarantees transits if you look for long enough, and hence we had derived a *time-infinite* transit probability. The numerical work also showed that transits frequently occurred within reasonable timeframes (\sim years). Applied to eclipsing binaries, the analytic work predicts that almost *all* circumbinary planets orbiting eclipsing binaries will eventually transit.

(ii) **This paper**: analytic derivation of the time-dependence of transitability, calculating when planets enter and exit it. By knowing the temporal windows of transitability, it advances the work in [Martin & Triaud \(2015\)](#) and improves applicability to astronomers with less than infinite time available.

(iii) **Future work**: calculation of the efficiency of transitability at producing transits, ultimately, yielding a complete time-dependent transit probability. This task is made difficult by the high sensitivity of the transit sequence to orbital parameters, as explored in [Martin & Triaud \(2014\)](#), and the broad parameter space.

The calculations made in this paper are kept as general as possible, accounting for any binary and planet inclination. Even though planets have only been discovered to date around eclipsing binaries, most binaries do not eclipse. Even though only coplanar planets have been found to date, circumbinary planets have been suggested to become misaligned due to planet-planet scattering ([Chatterjee et al. 2008](#); [Smullen et al. 2016](#)) or under the influence of an outer third star ([Munoz & Lai 2015](#); [Martin et al. 2015](#); [Hamers et al. 2016](#)).

Circumbinary transit probabilities have also been analysed in two recent papers. [Li et al. \(2016\)](#) followed a similar vein to derive a time-dependent transit probability, but only for planets around eclipsing binaries. Their work was also viewed as an extension of [Martin & Triaud \(2015\)](#). The primary purpose was to de-bias the observed trends in circumbinary planets to uncover their architectures. It was done using a Bayesian framework and with more rigour than the earlier study in [Martin & Triaud \(2014\)](#). [Brakensiek & Ragozzine \(2016\)](#) developed the semi-analytic algorithm CORBITS¹ to calculate the transit probability of any pairs of bodies, with primary applications to the *Kepler* multi-planet systems and the Solar System. Their algorithm has an orders of magnitude speed increase compared with N-body Monte Carlo simulations. It may be applied to circumbinary planets, but with the caveat it does

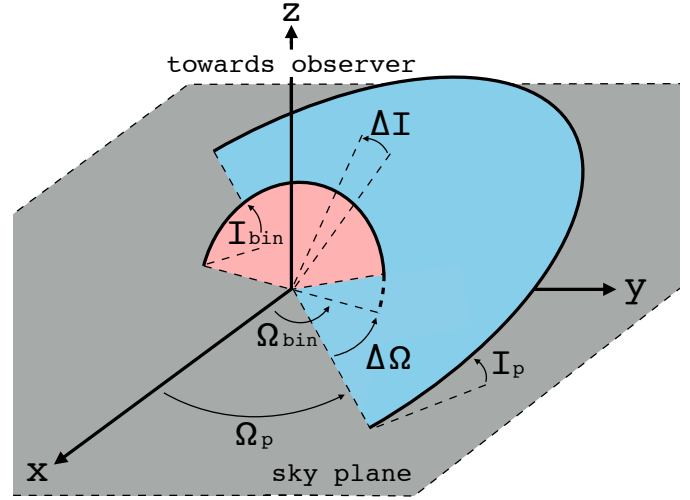


Figure 1. A misaligned circumbinary planet (blue, outer) orbiting a binary star system (pink, inner). The observer is looking down the positive z-axis (from above) so the x-y plane is the plane of the sky. The misalignment between the planet and binary orbits is characterised by the mutual inclination, ΔI (Eq. 1) and the mutual longitude of the ascending node, $\Delta \Omega$ (Eq. 2). Figure has been reproduced from [Martin & Triaud \(2015\)](#).

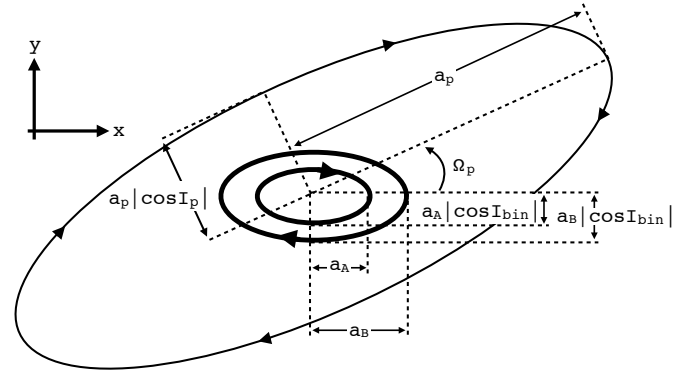


Figure 2. Orbits of a circumbinary planet and binary stars A and B, projected onto the x-y plane of the sky. To simplify the geometry, we have arbitrarily taken $\Omega_{\text{bin}} = 0$.

not account for precession of the planet’s orbital plane, which becomes important for long observing timespans such as the four-year *Kepler* mission.

This present paper is sliced up as follows. First, in Sect. 2 we setup the circumbinary geometry and orbital dynamics to be used. Following this in Sect. 3 is the analytic calculation of the time-dependence of transitability. In Sect. 4 we analyse the derived equations and some of the assumptions used. Finally, in Sect. 5 we apply our work to the known transiting circumbinary planets discovered by the *Kepler* mission and predict transits to be observed by future space missions, before concluding.

2 PROBLEM SETUP

2.1 Geometry

A circumbinary system is defined by two inner stars, of mass and radius $M_{A,B}$ and $R_{A,B}$, where we use “A” and “B” to denote the pri-

¹ Freely available at <https://github.com/jbrakensiek/CORBITS>.

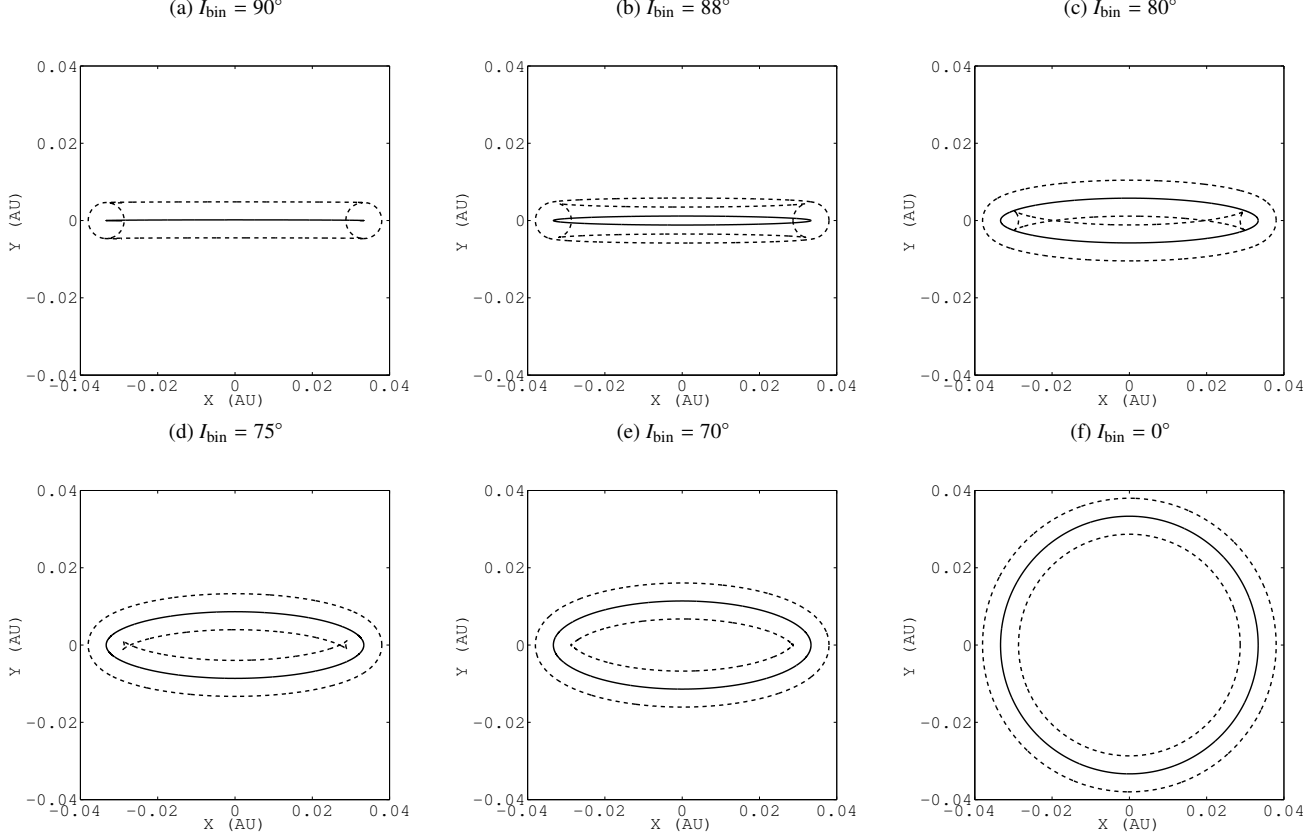


Figure 3. Projected primary stellar orbits on the x - y sky plane for $a_{\text{bin}} = 0.1$ AU, $R_A = 1R_\odot$, $M_A = 1M_\odot$, $M_B = 0.5M_\odot$ and six different values of I_{bin} . The solid line in the middle is the binary ellipse (Eq. 8). The outer and inner dashed lines show the full extent of the moving stellar disc, using Eqs. 9 and 10, respectively. The limiting case of a perfectly edge-on orbit in (a, $I_{\text{bin}} = 90^\circ$) is described by Eqs. 13 and 14, except for the rounded edges that these limiting equations do not account for. The limiting case of a perfectly face-on orbit in (f, $I_{\text{bin}} = 0^\circ$) is described by Eqs. 11 and 12. In (e) $I_{\text{bin}} = 70^\circ$ and this is roughly where the orbital extent starts to look like an annulus.

primary and secondary stars, and an outer planet with mass and radius M_p and R_p . The system is characterised using two Keplerian orbits, one for the binary and one for the planet orbiting the binary’s centre of mass, defined by osculating Jacobi elements. The planet and binary orbits are each defined by six orbital elements, which are chosen to be the semi-major axis, a , eccentricity, e , inclination, I , longitude of the ascending node, Ω , argument of periape, ω and true longitude, θ . Sometimes instead of a the orbital period is used, which we denote with T . A “p” subscript is used to denote planet quantities. For the binary, we either use “bin” for quantities general to both stars or “A” and “B” for quantities to specific to each individual star.

In Fig. 1 we illustrate an example circumbinary system where the planetary orbit (blue, outer) is misaligned to the binary orbit (pink, inner) by

$$\cos \Delta I = \cos \Delta \Omega \sin I_{\text{bin}} \sin I_p + \cos I_{\text{bin}} \cos I_p, \quad (1)$$

where the mutual longitude of the ascending node is

$$\Delta \Omega = \Omega_{\text{bin}} - \Omega_p. \quad (2)$$

In this geometry, an eclipsing binary has $I_{\text{bin}} \approx 90^\circ$. As an observer, we are only sensitive to $\Delta \Omega$ and not the two individual longitudes, and hence we may arbitrarily take $\Omega_{\text{bin}} = 0$ for simplicity.

The planet is assumed to have zero mass, since this outer body has a negligible effect on the orbital dynamics as long as it is roughly within the planetary regime (see Migaszewski & Goździewski (2011) and Martin & Triaud (2016) for more detail). The planet radius is also taken to be zero, since it generally has a negligible effect on the transit probabilities. Finally, for the geometry both binary and planetary orbits are assumed to be circular, but the effects of including eccentricity are analysed in Sect. 4.5.

The primary and secondary star orbits project an ellipse on the (x, y) plane of the sky:

$$\frac{x_{A,B}^2}{a_{A,B}^2} + \frac{y_{A,B}^2}{a_{A,B}^2 \cos^2 I_{\text{bin}}} = 1, \quad (3)$$

where

$$a_A = a_{\text{bin}} \frac{M_B}{M_A + M_B} \quad \text{and} \quad a_B = a_{\text{bin}} \frac{M_A}{M_A + M_B} \quad (4)$$

are the semi-major axes of the two individual stars. The planet similarly projects an ellipse on the sky,

$$\frac{(x_p \cos \Omega_p + y_p \sin \Omega_p)^2}{a_p^2} + \frac{(x_p \sin \Omega_p - y_p \cos \Omega_p)^2}{a_p^2 \cos^2 I_p} = 1, \quad (5)$$

4 Martin

but unlike the binary orbit, the ellipse defining the planetary orbit is rotated anti-clockwise on the plane of the sky by the angle Ω_p .

Equation 3 tracks the motion of the centre of each star, but for transits the motion of the each stellar disc is important. To define that we use offset curves, also known as parallel curves (Yates 1952). For a parametric curve

$$\begin{bmatrix} x \\ y \end{bmatrix} = \begin{bmatrix} f(\theta) \\ g(\theta) \end{bmatrix}, \quad (6)$$

where $f(\theta)$ and $g(\theta)$ are some arbitrary functions, the two branches of the offset curve at a distance k are

$$\begin{bmatrix} x_{\text{offset}} \\ y_{\text{offset}} \end{bmatrix} = \begin{bmatrix} f \pm \frac{kg'}{\sqrt{f'^2 + g'^2}} \\ g \mp \frac{kf'}{\sqrt{f'^2 + g'^2}} \end{bmatrix} \quad (7)$$

To calculate the binary offset curves, first convert Eq. 3 into a parametric equation of the true longitude $\theta_{A,B}$:

$$\begin{bmatrix} x_{A,B} \\ y_{A,B} \end{bmatrix} = \begin{bmatrix} a_{A,B} \cos \theta_{A,B} \\ a_{A,B} |\cos I_{\text{bin}}| \sin \theta_{A,B} \end{bmatrix}, \quad (8)$$

where $\theta_B = \theta_A + 180^\circ$ are the orbital phases of the individual stars. The outer offset curve, defined to be $R_{A,B}$ perpendicularly outwards from Eq. 8 for all $\theta_{A,B}$, is

$$\begin{bmatrix} x_{A,B,\text{outer}} \\ y_{A,B,\text{outer}} \end{bmatrix} = \begin{bmatrix} \left(a_{A,B} + \frac{|\cos I_{\text{bin}}| R_{A,B}}{\sqrt{\sin^2 \theta_{A,B} + \cos^2 I_{\text{bin}} \cos^2 \theta_{A,B}}} \right) \cos \theta_{A,B} \\ \left(a_{A,B} |\cos I_{\text{bin}}| + \frac{R_{A,B}}{\sqrt{\sin^2 \theta_{A,B} + \cos^2 I_{\text{bin}} \cos^2 \theta_{A,B}}} \right) \sin \theta_{A,B} \end{bmatrix}. \quad (9)$$

The inner curve is described by

$$\begin{bmatrix} x_{A,B,\text{inner}} \\ y_{A,B,\text{inner}} \end{bmatrix} = \begin{bmatrix} \left(a_{A,B} - \frac{|\cos I_{\text{bin}}| R_{A,B}}{\sqrt{\sin^2 \theta_{A,B} + \cos^2 I_{\text{bin}} \cos^2 \theta_{A,B}}} \right) \cos \theta_{A,B} \\ \left(a_{A,B} |\cos I_{\text{bin}}| - \frac{R_{A,B}}{\sqrt{\sin^2 \theta_{A,B} + \cos^2 I_{\text{bin}} \cos^2 \theta_{A,B}}} \right) \sin \theta_{A,B} \end{bmatrix}, \quad (10)$$

which differs from the outer curve only by a negative sign before the fraction, but this imposes a significant change. To better understand Eqs. 9 and 10, consider two limiting cases. When $I_{\text{bin}} = 0^\circ$ the orbit is face on and the outer and inner offset curves reduce to

$$\begin{bmatrix} x_{A,B,\text{outer}} \\ y_{A,B,\text{outer}} \end{bmatrix}_{I_{\text{bin}}=0^\circ} = \begin{bmatrix} (a_{A,B} + R_{A,B}) \cos \theta_{A,B} \\ (a_{A,B} + R_{A,B}) \sin \theta_{A,B} \end{bmatrix} \quad (11)$$

and

$$\begin{bmatrix} x_{A,B,\text{inner}} \\ y_{A,B,\text{inner}} \end{bmatrix}_{I_{\text{bin}}=0^\circ} = \begin{bmatrix} (a_{A,B} - R_{A,B}) \cos \theta_{A,B} \\ (a_{A,B} - R_{A,B}) \sin \theta_{A,B} \end{bmatrix}, \quad (12)$$

respectively, which expectedly describes a circular ring of outer diameter $2(a_{A,B} + R_{A,B})$ and thickness $2R_{A,B}$. In the other limit of $I_{\text{bin}} = 90^\circ$, i.e. a perfectly edge-on eclipsing binary, the offset curves reduce to

$$\begin{bmatrix} x_{A,B,\text{outer}} \\ y_{A,B,\text{outer}} \end{bmatrix}_{I_{\text{bin}}=90^\circ} = \begin{bmatrix} a_{A,B} \cos \theta_{A,B} \\ R_{A,B} \end{bmatrix} \quad (13)$$

and

$$\begin{bmatrix} x_{A,B,\text{inner}} \\ y_{A,B,\text{inner}} \end{bmatrix}_{I_{\text{bin}}=90^\circ} = \begin{bmatrix} a_{A,B} \cos \theta_{A,B} \\ -R_{A,B} \end{bmatrix}, \quad (14)$$

which expectedly describe a rectangle of length $2a_{A,B}$ and height $2R_{A,B}$. For I_{bin} at least $\sim 20^\circ$ away from 90° the orbital extent roughly resembles an annulus. In Fig. 3 are several examples of the extent of the stellar orbit.

Since the planet is assumed to have negligible radius, comparable offset curves are not calculated. A planet is in transitability when its projected orbital ellipse (Eq. 5) intersects the outer edge of the stellar orbit (Eq. 9). The inner offset curve plays no part in determining transitability.

2.2 Orbital Dynamics

Since we are considering a small outer body, the inner binary orbit is unperturbed, so we can take all of its orbital elements to be constant, except for its orbital phase. Contrastingly, the outer planetary orbit receives significant perturbations from the binary. According to Schneider (1994); Farago & Laskar (2010); Doolin & Blundell (2011) the orbital plane of the planet precesses around that of the binary at a constant rate, with period

$$T_{\text{prec}} = \frac{4}{3} \left(\frac{T_p^7}{T_{\text{bin}}^4} \right)^{1/3} \frac{(M_A + M_B)^2 (1 - e_p^2)^2}{M_A M_B \cos \Delta I}, \quad (15)$$

whilst maintaining a constant mutual inclination, ΔI . For any ΔI circumbinary planets can have stable orbits (Pilat-Lohinger et al. 2003; Doolin & Blundell 2011) and high-eccentricity Kozai-Lidov cycles are not applicable (Martin & Triaud 2016). Even though in this paper we consider circular binaries and planets when deriving the geometry of transitability, we can at least include planet eccentricity in calculating the precession period. Aside for a slight change to the timescale, the orbital precession behaves the same. Contrarily, if the binary is eccentric it induces some variations in ΔI , in addition to changing the timescale. The precession timescale of planets around eccentric binaries was derived by Farago & Laskar (2010) and is a more complicated function which we do not reproduce here. The effect on time-dependent transitability by assuming circular orbits is briefly investigated in Sect. 4.5, but fully incorporating the geometry and dynamics of eccentric orbits is a future task.

For constant ΔI , as the orbital plane of the planet rotates $I_p(t)$ and $\Omega_p(t)$ vary, whilst a_p is constant. The inclination of the planet on the plane of the sky, owing to this precession, follows a sinusoidal path

$$I_p(t) = \Delta I \cos \left(\frac{2\pi}{T_{\text{prec}}} (t - t_0) \right) + I_{\text{bin}}, \quad (16)$$

where $I_{p,0}$ is the initial planetary inclination at time t_0 ,

$$t_0 = -S \frac{T_{\text{prec}}}{2\pi} \cos^{-1} \left(\frac{I_{p,0} - I_{\text{bin}}}{\Delta I} \right), \quad (17)$$

where the factor $S = -1$ if $\Omega_{p,0}$ is between 0 and 180° and $S = +1$ if $\Omega_{p,0}$ is between 180 and 360° , where $\Omega_{p,0}$ is the initial planetary longitude of the ascending node. By inverting Eq. 2 and substituting in Eq. 1 the time-dependent equation for $\Omega_p(t)$ is

$$\Omega_p(t) = -\cos^{-1} \left(\frac{\cos \Delta I - \cos I_{\text{bin}} \cos I_p(t)}{\sin I_{\text{bin}} \sin I_p(t)} \right), \quad (18)$$

Throughout this paper as emphasis we always state the explicit time-dependence of $I_p(t)$ and $\Omega_p(t)$.

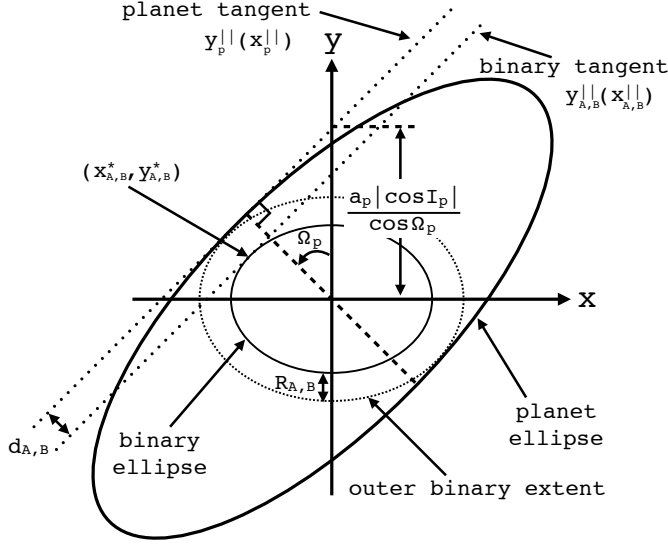


Figure 4. Illustration of the geometric definition of $d_{A,B}(t)$, the minimum distance between the planet and binary ellipses for a given orientation. Only one stellar orbit is shown, where we plot both the ellipse tracing out the centre of the star (solid line) and the outer offset curve (narrow dashed line). The dotted tangent lines correspond to Eq. 22 for the planet and Eq. 28 for the binary. In this example, the planet is on the edge of transitivity, and hence $d_{A,B}(t) = R_{A,B}$.

3 DERIVATION OF TIME-DEPENDENT TRANSITABILITY

Transitability occurs when the planetary ellipse (Eq. 5) intersects the outer edge of the binary orbit (Eq. 9). An exact solution of this would require finding solutions to

$$x_{A,B,\text{outer}}(\theta_{A,B}) = x_p(\theta_p) \quad \text{and} \quad y_{A,B,\text{outer}}(\theta_{A,B}) = y_p(\theta_p). \quad (19)$$

Calculating such intersections is not analytically feasible given the complicated functional form of the outer binary extent. Instead, simple geometric approach is employed which avoids explicit use of Eq. 9.

For configurations where the planet and stellar orbits do not intersect, we know that the distance between the planet and binary ellipses is minimised when the derivatives are equal:

$$\frac{dy_{A,B}}{dx_{A,B}}(\theta_{A,B}) = \frac{dy_p}{dx_p}(\theta_p). \quad (20)$$

We define this minimum distance as $d_{A,B}(t)$, where the time-dependence is indicative of the planet's dynamical evolution changing its orbital orientation. A planet is inside transitivity on the primary and/or secondary star at time t when

$$d_{A,B}(t) < R_{A,B}. \quad (21)$$

To calculate $d_{A,B}(t)$ we first approximate the planet orbit by a tangential line with a gradient $\tan \Omega_p(t)$, characterised by the function

$$y_p^|| = \tan \Omega_p(t) x_p^|| + \frac{a_p |\cos I_p(t)|}{\cos \Omega_p(t)}, \quad (22)$$

where the geometry of this equation is shown in Fig. 4. This is a

valid approach for a planet near the edge of transitivity, as long as the planet orbit is sufficiently larger than the stellar orbits. Fortunately, dynamical stability constraints dictate that $a_p \gtrsim 3a_{A,B}$ (Dvorak 1986; Dvorak et al. 1989; Holman & Wiegert 1999), which is sufficient to make the approximation valid.

The next step is to calculate the tangent equation to the binary ellipse with the same gradient $\tan \Omega_p(t)$. The distance between these two parallel lines corresponds to $d_{A,B}(t)$, also illustrated in Fig. 4. This diagram also illustrates the origin of the last part of Eq. 22.

To calculate the binary tangent line, first find the point on the binary orbit ellipse, $(x_{A,B}^*, y_{A,B}^*)$, where $dy_{A,B}/dx_{A,B} = \tan \Omega_p(t)$. Differentiate Eq. 3 with respect to $x_{A,B}$:

$$\frac{2x_{A,B}}{a_{A,B}^2} + \frac{2y_{A,B}}{a_{A,B}^2 \cos^2 I_{\text{bin}}} \frac{dy_{A,B}}{dx_{A,B}} = 0. \quad (23)$$

Evaluating Eq. 23 at $dy_{A,B}/dx_{A,B} = \tan \Omega_p(t)$ and re-arranging yields an expression relating $y_{A,B}^*$ and $x_{A,B}^*$:

$$y_{A,B}^* = -x_{A,B}^* \frac{\cos^2 I_{\text{bin}}}{\tan \Omega_p(t)}. \quad (24)$$

Substitute the expression for $y_{A,B}^*$ in Eq. 24 into the binary ellipse in Eq. 3 and solve for $x_{A,B}^*$:

$$x_{A,B}^* = \frac{-a_{A,B}}{\sqrt{1 + \frac{\cos^2 I_{\text{bin}}}{\tan^2 \Omega_p(t)}}}, \quad (25)$$

where we have taken the negative root to match the diagram in Fig. 4. Substitute Eq. 25 for $x_{A,B}^*$ into Eq. 24 and solve for $y_{A,B}^*$:

$$y_{A,B}^* = \frac{a_{A,B} \cos^2 I_{\text{bin}}}{\tan \Omega_p(t) \sqrt{1 + \frac{\cos^2 I_{\text{bin}}}{\tan^2 \Omega_p(t)}}}. \quad (26)$$

Now calculate the tangent line $y_{A,B}^||(\mathbf{x}_{A,B}^||)$ using

$$y_{A,B}^|| - y_{A,B}^* = \tan \Omega_p(t) (x_{A,B}^|| - x_{A,B}^*)$$

$$y_{A,B}^|| - \frac{a_{A,B} \cos^2 I_{\text{bin}}}{\tan \Omega_p(t) \sqrt{1 + \frac{\cos^2 I_{\text{bin}}}{\tan^2 \Omega_p(t)}}} = \tan \Omega_p(t) \left(x_{A,B}^|| + \frac{a_{A,B}}{\sqrt{1 + \frac{\cos^2 I_{\text{bin}}}{\tan^2 \Omega_p(t)}}} \right). \quad (27)$$

Rearrange to form the final binary tangent equation:

$$y_{A,B}^|| = \tan \Omega_p(t) x_{A,B}^|| + a_{A,B} \sqrt{\tan^2 \Omega_p(t) + \cos^2 I_{\text{bin}}}. \quad (28)$$

The planet tangent equation (Eq. 22) and binary tangent equation (Eq. 28) are parallel. The shortest distance between two parallel lines $y_1 = mx_1 + c_1$ and $y_2 = mx_2 + c_2$ is

$$\frac{c_2 - c_1}{\sqrt{m^2 + 1}}. \quad (29)$$

The distance between the two parallel lines in Eqs. 22 and 28 is $d_{A,B}(t)$, which we calculate to be

$$d_{A,B}(t) = \frac{\frac{a_p |\cos I_p(t)|}{\cos \Omega_p(t)} - a_{A,B} \sqrt{\tan^2 \Omega_p(t) + \cos^2 I_{\text{bin}}}}{\sqrt{\tan^2 \Omega_p(t) + 1}}, \quad (30)$$

which we simplify to

$$d_{A,B}(t) = a_p |\cos I_p(t)| - a_{A,B} \cos \Omega_p(t) \sqrt{\tan^2 \Omega_p(t) + \cos^2 I_{\text{bin}}}. \quad (31)$$

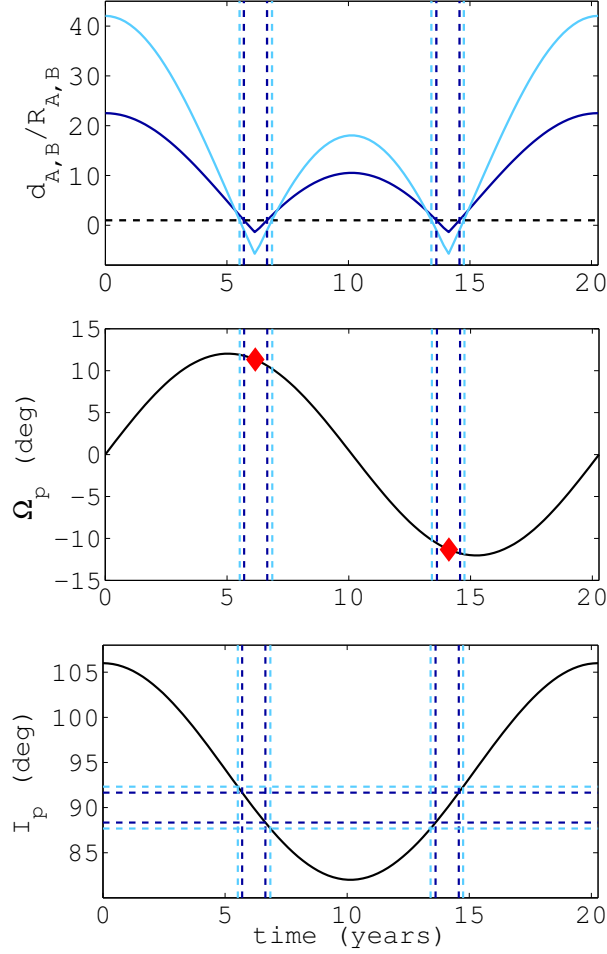


Figure 5. Calculation of the window of transitivity for an example circumbinary system: $M_A = 1M_\odot$, $M_B = 0.5M_\odot$, $R_A = 1R_\odot$, $R_B = 1R_\odot$, $a_{\text{bin}} = 0.1 \text{ AU}$, $a_p = 0.4 \text{ AU}$, $I_{\text{bin}} = 94^\circ$, $\Delta I = 12^\circ$ and $\Omega_p(t=0) = 0$. In all three figures the dark and light blue vertical lines denote the analytically-calculated regions in time when the planet is in transitivity on the primary and secondary stars, respectively. In the top image the minimum distance $d_{A,B}$ (Eq. 35) is plotted, scaled by the primary and secondary radii. The black horizontal dashed line is at $d_{A,B}/R_{A,B} = 1$, and hence below this limit transitivity occurs. Negative values occur when the planet and binary ellipses intersect. In the middle image the red triangles denote the approximately constant value of Ω_p when in transitivity (Eq. 32). In the bottom image the horizontal dashed lines denote the limits of transitivity in terms of I_p (Eq. 34).

It is not possible to analytically solve the inequality Eq. 21 with this expression for $d_{A,B}(t)$ due to the multiple instances of t so a simplification is needed. Transitivity occurs when I_p is near 90° . Applying this to Eq. 18, we approximate Ω_p in transitivity as a constant value

$$\Omega_p|_{\text{transitivity}} \approx -\cos^{-1}\left(\frac{\cos \Delta I}{\sin I_{\text{bin}}}\right). \quad (32)$$

Insert this approximation into Eq. 31 to obtain

$$d_{A,B}(t) = a_p |\cos I_p(t)| - a_{A,B} \frac{\cos \Delta I}{\sin I_{\text{bin}}} \sqrt{\tan^2 \left[\cos^{-1} \left(\frac{\cos \Delta I}{\sin I_{\text{bin}}} \right) \right] + \cos^2 I_{\text{bin}}}. \quad (33)$$

With only one instance of t remaining in Eq. 35 the limits of transitivity at $d_{A,B} = R_{A,B}$, in terms of the planet sky inclination, can be solved for:

$$I_p|_{\text{transitivity}} = \pm \cos^{-1} \left[\frac{R_{A,B}}{a_p} + \frac{a_{A,B}}{a_p} \frac{\cos \Delta I}{\sin I_{\text{bin}}} \right] \times \sqrt{\tan^2 \left(\cos^{-1} \left[\frac{\cos \Delta I}{\sin I_{\text{bin}}} \right] \right) + \cos^2 I_{\text{bin}}}. \quad (34)$$

The corresponding times that transitivity is entered and exited simply come from solving Eq. 16 for t using Eq. 34. Depending on the parameters, there may be zero, one or two regions of transitivity within a precession period, and hence zero, two or four times t to solve for. In Fig. 5 we provide an example of the evolution of $d_{A,B}/R_{A,B}$, Ω_p and I_p over a precession period for a circumbinary planet that goes in and out of transitivity twice. The secondary star has a slightly greater window of transitivity in this example, because even though it has a smaller radius, it sweeps out a larger area on the sky since $a_B = 2a_A$ here. Secondary star transitivity is usually longer except for eclipsing binaries.

In the limit of $a_{A,B} \rightarrow 0$, i.e. when the binary is compacted to a single object, the limits of transitivity in Eq. 34 reduce to

$$\lim_{a_{A,B} \rightarrow 0} I_p|_{\text{transitivity}} = \pm \cos^{-1} \left(\frac{R_{A,B}}{a_p} \right), \quad (35)$$

which are the inclination limits for transits of a single star, as expected.

4 ANALYSIS

4.1 Will the planet ever reach transitivity?

In this section we reproduce the result of [Martin & Triaud \(2015\)](#) for time-independent transitivity. To know whether or not transitivity will occur at some unspecified point in the planet's orbital evolution, calculate $d_{A,B}(t)$ at the extrema of $I_p(t)$, which are simply $I_{\text{bin}} \pm \Delta I$. The corresponding values of Ω_p according to Eq. 18 are

$$\begin{aligned} \Omega_p|_{\text{extrema}} &= -\cos^{-1} \left(\frac{\cos \Delta I - \cos I_{\text{bin}} \cos(I_{\text{bin}} \pm \Delta I)}{\sin I_{\text{bin}} \sin(I_{\text{bin}} \pm \Delta I)} \right) \\ &= -\cos^{-1} \left(\frac{\cos \Delta I - \frac{1}{2} [\cos(I_{\text{bin}} - (I_{\text{bin}} \pm \Delta I)) + \cos(I_{\text{bin}} + (I_{\text{bin}} \pm \Delta I))]}{\frac{1}{2} [\cos(I_{\text{bin}} - (I_{\text{bin}} \pm \Delta I)) - \cos(I_{\text{bin}} + (I_{\text{bin}} \pm \Delta I))]} \right) \\ &= -\cos^{-1} \left(\frac{\cos \Delta I - \frac{1}{2} [\cos(\mp \Delta I) + \cos(2I_{\text{bin}} \pm \Delta I)]}{\frac{1}{2} [\cos(\mp \Delta I) - \cos(2I_{\text{bin}} \pm \Delta I)]} \right) \\ &= -\cos^{-1}(1) \\ &= 0, \end{aligned} \quad (36)$$

where we have used a prosthaphaeresis trigonometric identity between the first and second lines. The minimum value of $d_{A,B}(t)$, according to Eq. 31 with $\Omega_p|_{\text{extrema}} = 0$ and $I_p = I_{\text{bin}} - \Delta I$, is

$$d_{\text{min}} = a_p \sin \left| \frac{\pi}{2} - I_{\text{bin}} + \Delta I \right| - a_{A,B} \sin \left| \frac{\pi}{2} - I_{\text{bin}} \right|, \quad (37)$$

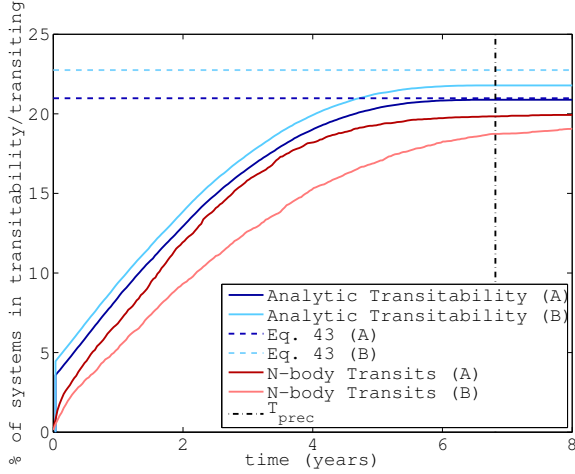


Figure 6. Transitivity and transit percentages over time for an example circumbinary system with $M_A = 1M_\odot$, $M_B = 0.5M_\odot$, $R_A = 1R_\odot$, $R_B = 0.5R_\odot$, $T_{\text{bin}} = 7$ d, $T_p = 40$ d and $\Delta I = 10^\circ$. In dark and light blue solid lines we plot the *time-dependent* probability of transitivity $P_{A,B}(t)$ as a percentage for the primary and secondary stars, respectively. In dark and light red solid lines we plot the percentage of systems found to be actually transiting at time t using an N-body code. The horizontal dashed blue lines at the top indicate the *time-independent* probability of transitivity from Eq. 43. Finally, the black vertically dot-dashed indicates $T_{\text{prec}} = 6.82$ yr.

where to match the notation of [Martin & Triaud \(2015\)](#) we use $|\cos I_{\text{bin}}| = \sin|\pi/2 - I_{\text{bin}}|$, which is valid for $I_{\text{bin}} \in [0^\circ, 180^\circ]$. For transitivity to occur at some point requires $d_{\text{min}} < R_{A,B}$. Inserting this condition into Eq. 37² yields

$$R_{A,B} > a_p \sin\left|\frac{\pi}{2} - I_{\text{bin}} + \Delta I\right| - a_{A,B} \sin\left|\frac{\pi}{2} - I_{\text{bin}}\right|, \quad (38)$$

which we re-arrange to form

$$R_{A,B} + a_{A,B} \sin\left|\frac{\pi}{2} - I_{\text{bin}}\right| > a_p \sin\left|\frac{\pi}{2} - I_{\text{bin}} + \Delta I\right|, \quad (39)$$

$$\sin^{-1}\left(\frac{R_{A,B} + a_{A,B} \sin\left|\frac{\pi}{2} - I_{\text{bin}}\right|}{a_p}\right) > \left|\frac{\pi}{2} - I_{\text{bin}} + \Delta I\right|, \quad (40)$$

$$\sin^{-1}\left(\frac{R_{A,B}}{a_p} + \frac{a_{A,B}}{a_p} \sin\left|\frac{\pi}{2} - I_{\text{bin}}\right|\right) - \left|\frac{\pi}{2} - I_{\text{bin}}\right| > \Delta I, \quad (41)$$

$$\Delta I > \left|\frac{\pi}{2} - I_{\text{bin}}\right| - \sin^{-1}\left(\frac{a_{A,B}}{a_p} \sin\left|\frac{\pi}{2} - I_{\text{bin}}\right| + \frac{R_{A,B}}{a_p}\right), \quad (42)$$

which recovers the *time-independent* transitivity criterion derived in [Martin & Triaud \(2015\)](#)³.

4.2 Time-dependent probability of transitivity

In [Martin & Triaud \(2015\)](#) we calculated that the probability of a circumbinary planet exhibiting transitivity at some unspecified point in time is

$$P_{A,B} = \sin\left(\Delta I + \frac{a_{A,B} \sin \Delta I + R_{A,B}}{a_p - a_{A,B} \cos \Delta I}\right), \quad (43)$$

² Note: we are not using the simplified version of $d_{A,B}(t)$ in Eq. 35.

³ Equations 18 and 19 in that paper, which use $\Delta I = |I_p - I_{\text{bin}}|$ when $\Omega_p = 0$.

where this equation assumes $\cos I_{\text{bin}}$ is uniformly distributed, and hence it covers both eclipsing and non-eclipsing binaries⁴. We may improve upon this by calculating $P_{A,B}(t)$ using the new time-dependent criteria for transitivity.

To calculate $P_{A,B}(t)$ we create a uniform distribution of $\cos I_{\text{bin}}$ and for each value of I_{bin} we choose a random t_0 between 0 and T_{prec} . With these two values and the other set system parameters we can analytically solve $I_p(t) = I_p|_{\text{transitivity}}$ for t and find the time the system first enters transitivity. The probability $P_{A,B}(t)$ is by definition the fraction of systems which have already entered transitivity by the time t . At $t = T_{\text{prec}}$ all systems that will ever enter transitivity will have already done so, at which point $P_{A,B}(t)$ should reach the value calculated in Eq. 43.

In Fig. 6 we show an example calculation for a circumbinary system with $M_A = 1M_\odot$, $M_B = 0.5M_\odot$, $R_A = 1R_\odot$, $R_B = 0.5R_\odot$, $T_{\text{bin}} = 7$ d, $T_p = 40$ d and $\Delta I = 10^\circ$. This is the same test as was done in Fig. 11 of [Martin & Triaud \(2015\)](#). For both primary and secondary stars we plot $P_{A,B}(t)$, transit probabilities calculated using an N-body code and $P_{A,B}$ coming from Eq. 43.

As expected, the curves of $P_{A,B}(t)$ are higher than the N-body transit probabilities. This is because transitivity is not 100% efficient at producing transits. The analytic and N-body curves are reasonably close for the primary star, implying a high efficiency of transitivity. On the other hand, transitivity is significantly less efficient on the secondary star, which is expected, since the secondary star is both physically smaller and it sweeps out a wider region of the sky, so it is easier for a planet to miss transits. The tricky process of calculating this analytic efficiency of transitivity is to be done in the third and final paper of this series. We note that the $P_{A,B}(t)$ curves do not start at zero at $t = 0$ because some systems begin in transitivity.

There is one problem evident in Fig. 6: the analytically calculated $P_{A,B}(t)$ at $t = T_{\text{prec}}$ does not quite reach the values calculated in Eq. 43. For the primary star (dark blue) this is barely noticeable but this small discrepancy is readily apparent for the secondary star (light blue). This small error is the result of the Eq. 32 approximation of constant Ω_p during transitivity, which was necessary to analytically derive the inclination limits for transitivity in Eq. 34. A way to avoid this error would be to test for transitivity by solving $d(t) < R_{A,B}$ directly using Eq. 31 without the approximation in Eq. 32. This would require a numerical algorithm, but would nevertheless be much faster still than a large suite of N-body simulations⁵.

4.3 Percentage of time spent in transitivity

Whether or not a planet spends a large amount of its time in transitivity or just has fleeting appearances has consequences on its detectability. As an example, the most misaligned circumbinary planet known to date is Kepler-413 with $\Delta I = 4.02^\circ$ ([Kostov et al.](#)

⁴ In the published version of [Martin & Triaud \(2015\)](#) this equation (Eq. 24 in that paper) contains a typo where the $-$ sign in the denominator is incorrectly a $+$ sign. Similarly, Eq. 22 of that paper has $+$ sign that should be a $-$ sign, and Eq. 23 has a $-$ sign that should be a $+$ sign. Those errors were purely typographical and the results presented throughout that paper were done using the correct formulae. Furthermore, the typos have been fixed in the arXiv version of the paper. We are sorry for the errors and any inconvenience caused.

⁵ For example, the N-body curves in Fig. 6 were calculated using a suite of 10,000 randomised circumbinary systems and required several hours to numerically integrate the orbits and calculate transit times.

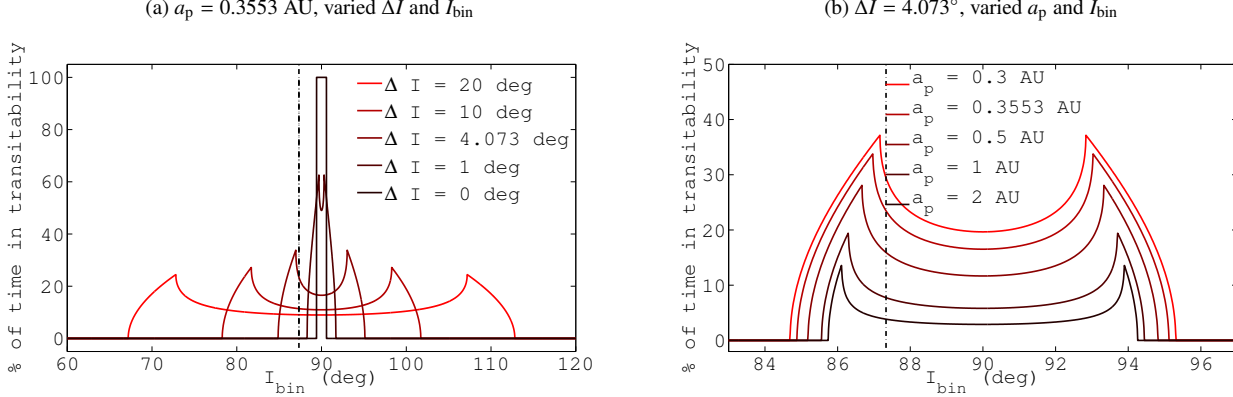


Figure 7. The analytically-calculated percentage of time that a planet spends in transitivity on the primary star as a function of I_{bin} . The orbital parameters are taken from Kepler-413 (Kostov et al. 2014): $M_A = 0.820M_\odot$, $M_B = 0.542M_\odot$, $R_A = 0.78R_\odot$, $a_{\text{bin}} = 0.10148$ AU, $a_p = 0.3553$ AU, $\Delta I = 4.073^\circ$. All values of I_{bin} outside of the plotted range have 0% transitivity. The true binary inclination $I_{\text{bin}} = 87.33^\circ$ is demarcated by a black vertical dot-dashed line. In a) we vary the mutual inclination from its nominal value, with the red to black colour gradient denoting a decreasing ΔI . In b) we instead value the planet semi-major axis, with the red to black colour gradient denoting an increasing a_p .

2014). It is also one of the tightest systems found, with $a_{\text{bin}} = 0.1$ AU and $a_p = 0.36$ AU, yielding a relatively short precession period of 11.1 yr. Near the beginning of the *Kepler* mission it transited three times, roughly 63 days apart, before disappearing for 838 days as the planet precessed out of transitivity. Such a system could be easily mistaken as a transient false positive, but luckily it returned for five more transits within the original *Kepler* mission. In fact, Kepler-413 only spends 23.5% and 24.0% of its time in transitivity on the primary and secondary stars, respectively.

In Fig. 7a we plot the percentage of time spent in transitivity as a function of I_{bin} , for a circumbinary system with the other parameters matching Kepler-413 (see Table 1), but with five different values of ΔI . For clarity, only primary transitivity is shown. As calculated in Martin & Triaud (2015), the amount of systems exhibiting transitivity (i.e. the range of I_{bin}) increases as ΔI increases. However, the new result is that for systems exhibiting transitivity, the percentage of time spent in transitivity generally decreases as ΔI increases. Only for ΔI very close to 0° is transitivity permanent, but this only applies for I_{bin} very close to 90° . For $I_{\text{bin}} = 87.33^\circ$, corresponding to the actual Kepler-413 system and demarcated by a black vertical dot-dashed line, a few degrees of mutual inclination is needed for transits to be possible; highly coplanar planets would never have been discovered.

In Fig. 7b we instead keep ΔI at its true value of 4.073° and vary a_p . For a_p between 0.3 and 2 AU there is not a significant difference in the range of I_{bin} centred on 90° that allows transitivity. This is in line with the weak period dependence found by Martin & Triaud (2015). However, the new result is that the percentage of time in transitivity is reduced as the planet is moved farther out. Distant planets may still transit but their photometric appearances are ephemeral. Furthermore, since $T_{\text{prec}} \propto T_p^{7/3}$, the time between these fleeting transit opportunities is appreciable. The one advantage of long period planets is that the efficiency of transitivity should be higher for the same period binary. This is because longer-period planets move at slower speeds ($v \approx 2\pi a/T$), so as the planet passes the binary the binary may cover more of its orbit and is hence less likely to be missed. The effect of this is to be quantified in the third and final paper of this series.

4.4 Accuracy of the precession period

Because transitivity is a sensitive function of $I_p(t)$, the time-dependence of transitivity is intrinsically linked to the precession period. Therefore, our ability to analytically predict windows of transitivity is reliant upon the accuracy of T_{prec} . An in-depth numerical critique of the analytic formulae from Farago & Laskar (2010) was done by Doolin & Blundell (2011), so here we just show two examples.

First, shown in Fig. 8a is the evolution of $I_p(t)$ for Kepler-16, calculated both analytically using Farago & Laskar (2010) (blue solid curves) and from N-body simulations (red dashed curves). Results are shown for both the true binary eccentricity $e_{\text{bin}} = 0.16$ (lighter coloured curves) and for $e_{\text{bin}} = 0$ (darker coloured curves). The planet eccentricity is set to the true value in all cases, but is a negligibly small $e_p = 0.0069$. All orbital parameters are listed in Table 1. Eccentric precession periods are, as predicted, shorter than for circular orbits. This is a small difference compared to the discrepancy of roughly 10% error between the longer analytic periods and shorter N-body periods.

Repeating the task for Kepler-34, which has the largest eccentricity of any of the known planet hosts at $e_{\text{bin}} = 0.521$, we see in Fig. 8b that there is a much more stark shortening of the precession period for the eccentric orbit. Furthermore, in this case we see a much better match of precession periods between the analytic and N-body solutions. There is, however, a small difference in the amplitude of the variation of $I_p(t)$ between analytic and N-body curves in the eccentric case. This is because in the N-body curve ΔI varies by an amplitude of $\sim 1^\circ$, whereas Eq. 16 assumes constancy.

It is speculated that that discrepancies in the precession period may arise from the formula being calculated using a quadrupole expansion of the Hamiltonian, and higher-order effects may account for the error. This is consistent with the Farago & Laskar (2010) quadrupole precession period working better for Kepler-34 than for Kepler-16, as the former has nearly equal mass binaries and hence the octupole perturbation on the planet is minimal. Fully quantifying this is left for future investigation.

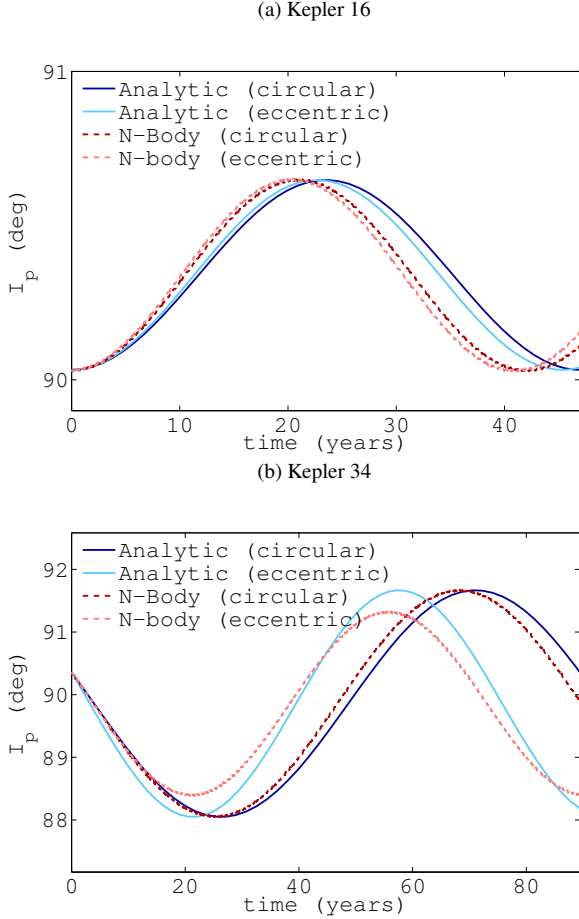


Figure 8. Time evolution of I_p for Kepler-16 (a) and Kepler-34 (b), calculated in four different ways: 1) dark blue, solid line: analytically using Eq. 15 assuming $e_{\text{bin}} = 0$; 2) light blue, solid line: analytically using equations in Farago & Laskar (2010) with $e_{\text{bin}} = 0.159$; 3) dark red, dashed line: numerically using N-body simulations and $e_{\text{bin}} = 0$ and 4) light red, dashed line: numerically using N-body simulations with $e_{\text{bin}} = 0.521$. In all cases e_p is set to the true value, not zero.

4.5 The effects of eccentric planets and binaries

The probability of a planet transiting a single star is often simply quoted as $P_{\text{single}} = R_{\text{star}}/a_p$, however when eccentricity is included Barnes (2007) modified the equation to

$$P_{\text{single}} = \frac{R_{\text{star}}}{a_p} \frac{1}{1 - e_p^2}, \quad (44)$$

which has been marginalised over all possible values of ω_p . Eccentricity gives a boost to transit probabilities around single stars.

If a circumbinary system has eccentric binary and/or planetary orbits, there are three effects on the transit probability. First, like in the single star case the geometry is complexified by the addition of extra orbital elements: e_{bin} , ω_{bin} , e_p and ω_p . The projected stellar orbits (e.g. Fig. 3) are no longer vertically symmetric and the planet orbit is no longer rotationally symmetric.

The second effect is that increased eccentricity in either the binary or planet orbit pushes the stability limit farther out (Holman & Wiegert 1999; Mardling & Aarseth 2001). For example, a planet with $a_p = 3a_{\text{bin}}$ is very close to the stability limit for circular orbits.

However, if the planet instead has a moderate eccentricity, say more than 0.2, then its transit probability may be increased but the orbit is likely unstable. To achieve stability a_p would have to be increased, likely offsetting any gain in the transit probability.

Finally, eccentricity affects the orbital dynamics. If $e_{\text{bin}} > 0$ then the assumption of constant ΔI is no longer valid and the planetary orbit precesses at a variable rate (Farago & Laskar 2010; Doolin & Blundell 2011). For $\Delta I \lesssim 45^\circ$ the precession is still prograde, but above this islands of libration appear and hence complicate matters further. If the planet is eccentric then ΔI remains constant and there are no islands of libration, but the constant precession period is decreased by a factor $(1 - e^2)^2$, as accounted for in Eq. 15. If the planet is eccentric then in addition to precession of Ω_p there will be an apsidal advance of ω_p at a nearly equal rate but in opposite directions (Lee & Peale 2007).

A full incorporation of the geometry and dynamics of eccentricity systems is a future task. Fortunately, it was already shown in Martin & Triaud (2015) that assuming circular orbits is generally reasonable for predicting if transitability occurs. In that paper N-body simulations of 10,000 circumbinary systems were integrated over an entire precession period to check if the planet and binary orbits ever overlapped. Orbital parameters were randomised within ranges roughly corresponding to the known systems. For eccentricity e_{bin} and e_p were independently randomised between 0 and 0.5. Predicting whether or not transitability occurred was shown to be accurate more than 98% of the time. Furthermore, it was found that slightly more systems entered transitability than expected when eccentricity was included, similar to the result for single stars in Eq. 44.

An additional example test was run to see the effect of eccentricity on time-dependent transitability. A base circumbinary system was created with $M_A = 1M_\odot$, $M_B = 0.5M_\odot$, $P_{\text{bin}} = 5$ d, $P_p = 85$ d, $a_{\text{bin}} = 0.065$ AU, $a_p = 0.43$ AU, $i_{\text{bin}} = 95^\circ$, $I_p = 100^\circ$, $\Omega_{\text{bin}} = 0^\circ$ and $\Omega_p = 5^\circ$. Both ω and θ for the binary and planet were initially set to 0° . Four simulations were run with e_{bin} and e_p set to either 0 or 0.4. In Fig. 9 is a plot of the variation of the orbital elements over time in the four simulations: both binary and planet orbits are initially eccentric (light blue), both are initially circular (light red), only the planet is eccentric (dark red) and only the binary is eccentric (dark blue). All plots have been normalised to the precession period. Detailing the complex orbital mechanics of circumbinary planets is beyond the scope of this work, and has been covered in various papers (e.g. Leung & Hoi Lee 2013; Georgakarakos & Eggl 2015), so here only a brief description of each variation is provided.

- **Eccentricity:** If the binary is circular then the planet, whether it be initially circular or initially eccentric, has a constant eccentricity. Conversely, an eccentric binary induces periodic variations in the planet's eccentricity of ~ 0.05 in magnitude.

- **Semi-Major Axis:** In all four cases the planet's semi-major axis does not vary by more than $\sim 5\%$. As both planet and binary eccentricities increase, the variation in a_p increases.

- **Argument of Periapse:** For initially eccentric planets ω_p has a simple behaviour between 0° and 360° , although if the binary is eccentric there is some slight non-linearity and the apsidal advance of ω_p is slightly faster than the precession of Ω_p . If both the planet and binary are circular then ω_p is essentially undefined, leading to the light red fuzz covering most of the plot. For an initially circular planet around an eccentric binary ω_p is initially undefined but becomes defined as e_p grows above zero under influence from the binary.

- **Longitude of the Ascending Node:** The behaviour of Ω_p is

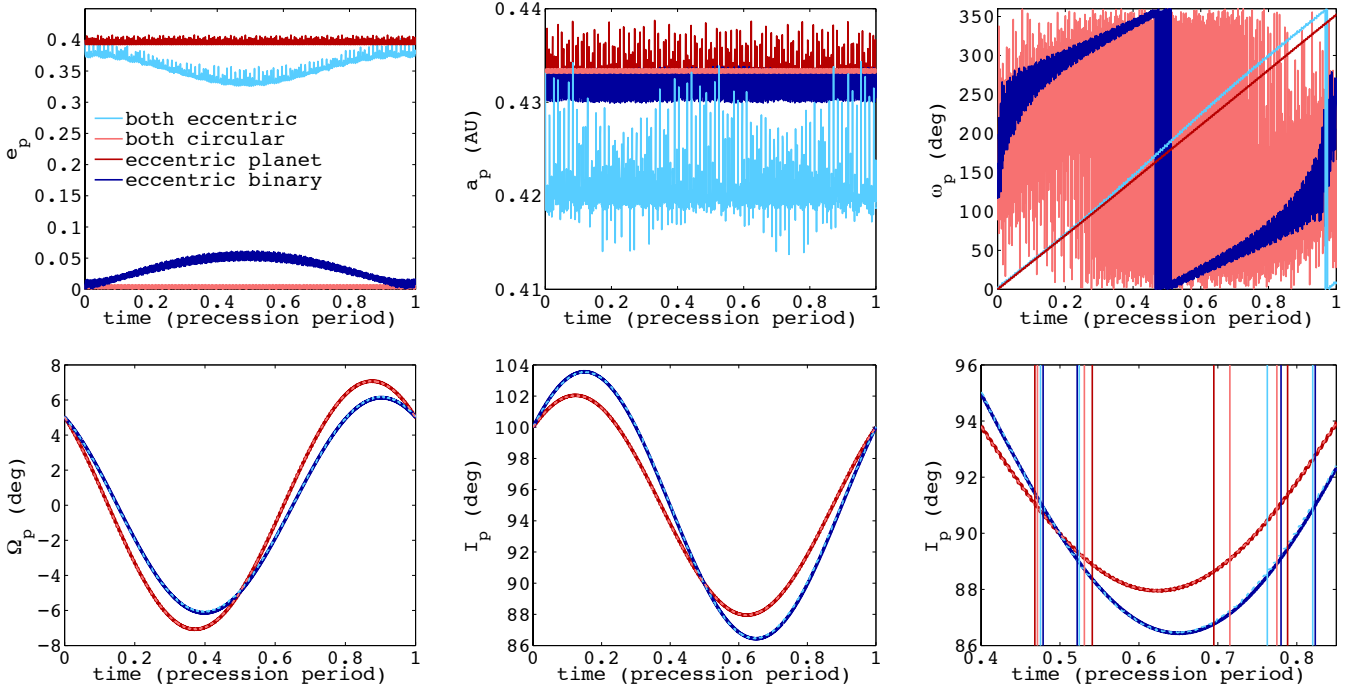


Figure 9. Variation of the orbital elements of a circumbinary planet over time according to four N-body simulations. Common to all four simulations are the starting conditions: $M_A = 1M_\odot$, $M_B = 0.5M_\odot$, $P_{\text{bin}} = 5$ d, $P_p = 85$ d, $a_{\text{bin}} = 0.065$ AU, $a_p = 0.43$ AU, $I_{\text{bin}} = 95^\circ$, $I_p = 100^\circ$, $\Omega_{\text{bin}} = 0^\circ$, $\Omega_p = 5^\circ$ and $\omega_{\text{bin}} = \omega_p = \theta_{\text{bin}} = \theta_p = 0^\circ$. The binary and planet eccentricities are initially set to either 0 or 0.4, and the four simulations are the different combinations of these eccentricities, shown in different colours outlined in the top left plot. In the bottom right plot is a zoomed version of the evolution of I_p with vertical lines denoting two windows of transitivity for each simulation. Note that for the curves on the bottom row the two red curves overlap and the two blue curves overlap as the orbital precession is a function of e_{bin} but not e_p . For this reason dashed lines are used.

dependent on e_{bin} and not e_p . Consequently, the light and dark red curves are overlapping (circular binaries) and the light and dark blue curves are overlapping (eccentric binaries). For an eccentric binary the sinusoid is slightly skewed to the right, indicative of the variable precession rate that [Farago & Laskar \(2010\)](#) and [Doolin & Blundell \(2011\)](#) discovered.

- **Inclination:** The most important parameter for transitivity is I_p . Similar to Ω_p , the variation of I_p only depends on e_{bin} and not e_p . For eccentric binaries (light and dark blue curves) we see that a greater range of I_p is covered. This is consistent with the tests of [Martin & Triaud \(2015\)](#) which showed eccentricity generally boosts the amount of planets in transitivity.

The bottom right plot in Fig. 9 is the variation of I_p zoomed to the windows of transitivity⁶, demarcated by vertical lines of the corresponding colour. There are two such windows, one centred around $0.5T_{\text{prec}}$ and one to the right. Since transitivity occurs when I_p is near 90° , we see that the windows are somewhat similar for the first window of transitivity. For the second window of transitivity they are spread out by $\sim 10\%$ of the precession period. The windows of transitivity tend to be longer for eccentric binaries (light and dark red curves) as a result of the smaller variation of I_p , as shown in Sect. 4.3.

A preliminary conclusion is that the predominant effect of eccentricity on transitivity is not how it changes the geometry but rather how it changes the orbital precession. In that sense, e_p has

negligible effect as the evolution of I_p is unaffected by it, whilst e_{bin} may be important. There is also evidence that eccentricity increases transit probabilities but this is yet to be fully quantified.

5 APPLICATIONS TO THE KNOWN *KEPLER* CIRCUMBINARY PLANETS

5.1 Predicted future transits and observations with *TESS*, *CHEOPS* and *PLATO*

To the interest of those wanting follow-up transit observations of the known *Kepler* transiting systems, this theory is applied to some upcoming photometric space missions. Whilst transit follow-up is possible from the ground, it is hampered in two ways. First, the known circumbinary planets all have 50+ day periods, considered long for transit studies. This makes scheduling difficult, particularly for ground-based observations. Second, transit durations of circumbinary planets (equation derived in [Kostov et al. 2014](#)) may be significantly longer than equivalent single-star transits, owing to the relative motion of the two stars, and hence may be longer than an observing night.

The upcoming photometric missions we apply our results to are listed below. The *K2* mission is not included as it has never re-observed the original *Kepler* field.

- **TESS:** A desired launch date of August 2017, after which *TESS* will observe the southern hemisphere for one year before observing the northern hemisphere for one year, starting roughly August 2018. Within this year, the original *Kepler* field is likely to receive roughly one or two months of time coverage.

⁶ So that eccentricity can be accounted for, these are calculated using N-body simulations and numerical tests of overlapping orbits.

Table 1. Orbital parameters of the transiting systems discovered so far by *Kepler*.

| Name | M_A (M_\odot) | M_B (M_\odot) | R_A (R_\odot) | R_B (R_\odot) | a (AU) | P (day) | e | I (deg) | Ω (deg) | ω (deg) | λ (deg) | ΔI (deg) | Epoch (BJD) |
|---------------|------------------------|------------------------|------------------------|------------------------|-------------|--------------|-------|--------------|-------------------|-------------------|--------------------|---------------------|----------------|
| 16 Binary | 0.690 | 0.203 | 0.649 | 0.226 | 0.224 | 41.079 | 0.159 | 90.340 | 0 | 263.464 | 92.352 | - | 2,455,212.123 |
| 16 Planet b | - | - | - | - | 0.705 | 228.776 | 0.007 | 90.032 | 0.003 | 318 | 106.51 | 0.308 | |
| 34 Binary | 1.048 | 1.021 | 1.162 | 1.093 | 0.229 | 27.796 | 0.521 | 89.858 | 0 | 71.436 | 300.197 | - | 2,454,969.200 |
| 34 Planet b | - | - | - | - | 1.090 | 288.822 | 0.182 | 90.355 | -1.74 | 7.907 | 106.5 | 1.810 | |
| 35 Binary | 0.888 | 0.809 | 1.028 | 0.786 | 0.176 | 20.734 | 0.142 | 90.424 | 0 | 86.513 | 89.178 | - | 2,454,965.850 |
| 35 Planet b | - | - | - | - | 0.604 | 131.458 | 0.042 | 90.76 | -1.24 | 64.093 | 136.4 | 1.285 | |
| 38 Binary | 0.949 | 0.249 | 1.757 | 0.272 | 0.147 | 18.795 | 0.103 | 89.265 | 0 | 268.680 | 236.733 | - | 2,454,970.0 |
| 38 Planet b | - | - | - | - | 0.464 | 105.595 | 0.032 | 89.446 | -0.012 | 32.829 | 37.817 | 0.181 | |
| 47 Binary | 1.043 | 0.362 | 0.964 | 0.351 | 0.084 | 7.448 | 0.023 | 89.34 | 0 | 212.3 | 235.85 | - | 2,455,000.0 |
| 47 Planet b | - | - | - | - | 0.296 | 49.514 | 0.094 | 89.59 | 0.1 | 178.172 | 350.589 | 0.269 | |
| 47 Planet c | - | - | - | - | 0.989 | 303.158 | 0.423 | 89.826 | 1.06 | 214.104 | 305.164 | 1.166 | |
| 64 Binary | 1.384 | 0.336 | 1.734 | 0.378 | 0.174 | 20.000 | 0.212 | 87.360 | 0 | 217.6 | 291.6 | - | 2,454,900.0 |
| 64 Planet b | - | - | - | - | 0.634 | 138.506 | 0.054 | 90.022 | 0.89 | 348.0 | 186.90 | 2.807 | |
| 413 Binary | 0.820 | 0.542 | 0.776 | 0.484 | 0.101 | 10.116 | 0.037 | 87.322 | 0 | 279.74 | 62.887 | - | 2,455,000.0 |
| 413 Planet b | - | - | - | - | 0.355 | 66.262 | 0.118 | 89.929 | 3.139 | 94.6 | 0.5 | 4.073 | |
| 453 Binary | 0.934 | 0.194 | 0.833 | 0.214 | 0.185 | 27.322 | 0.052 | 90.266 | 0 | 263.049 | 72.241 | - | 2,454,964.0 |
| 453 Planet b | - | - | - | - | 0.788 | 240.503 | 0.036 | 89.443 | 2.103 | 185.149 | 299.039 | 2.298 | |
| 1647 Binary | 1.221 | 0.968 | 1.790 | 0.966 | 0.278 | 11.259 | 0.160 | 87.916 | 0 | 300.544 | 31.716 | - | 2,455,000.0 |
| 1647 Planet b | - | - | - | - | 2.721 | 1107.592 | 0.058 | 90.097 | -2.039 | 155.046 | 94.3780 | 3.016 | |

Refs: Doyle et al. (2011); Welsh et al. (2012, 2014); Orosz et al. (2012a,b); Schwamb et al. (2013); Kostov et al. (2013, 2014, 2016).

Note: Updated elements for Kepler-453 and -1647 provided by Veselin Kostov (priv. comm.).

Note: λ is the mean longitude.

Note: Kepler-47d is excluded because it has not yet been published and lacks a value for ΔI .

Note: Kepler-64 is also known as PH-1, as it was discovered by the Planet Hunters consortium: <https://www.planethunters.org/>

• **CHEOPS:** A desired launch date of December 2017 and a nominal 3.5 yr mission. Unlike the other missions, *CHEOPS* is not a transit survey for new planets but primarily a follow-up photometric space mission to better characterise known planets. In its low-Earth orbit, it has optimal observability of stars near the ecliptic. The *Kepler* field is observable but near the limit.

• **PLATO:** A desired launch date of early 2024 and a nominal 6 yr mission. The schedule of *PLATO* is unlikely to be decided until just a few years before launch, and will likely consist of many short observing fields, running for a few months, and one or two extended views, running for a one or multiple years. It is almost certain that the *Kepler* field will be re-observed at some time but it is not known when and for how long.

The orbital parameters of the known circumbinary planets are listed in Table 1. For each system we calculate $I_p(t)$ and the limits of transitivity, $I_p|_{\text{transitivity}}$. The timing of actual transits on the primary and secondary stars is calculated using an N-body code. In light of the slight errors in the analytically calculated precession period (Sect. 4.4), we use here the “true” precession period which is taken from the N-body simulation. In Figs. 10 and 10 we show our results over 20 years between 2013 and 2033. This timespan covers the end of the original *Kepler* mission up until a few years past the future *PLATO* mission.

For each of the systems we summarise their observability in Table 2, where a ✓ indicates transitivity predicted by the analytic formula on the primary or secondary star and the number in brackets is the amount of transits found in the N-body simulation. The

“predicted extra planets” column is explained in Sect. 5.2. Individual remarks on each system are provided below.

• **Kepler-16:** Unobservable except on the primary at the very start of *CHEOPS*, although this 2018 transit is predicted to be very grazing, with a duration of roughly one hour.

• **Kepler-34:** The windows of transitivity are nearly identical for the primary and secondary stars, owing to their similar mass and radius. The N-body code shows a transit in 2015 that occurs despite $I_p(t)$ being outside the window of transitivity. This is caused by the highly eccentric binary orbit ($e_{\text{bin}} = 0.52$), which was shown in Sect. 4.5 to shift the windows of transitivity.

• **Kepler-35:** A good *CHEOPS* and *TESS* target, but illusive to the nominal *PLATO* mission.

• **Kepler-38:** The only known circumbinary planet with permanent transitivity on the primary star, visible for all time. Contrastingly though, it will never transit the secondary star.

• **Kepler-47b:** The innermost planet in the three-planet system has primary transits that are fully observable by *TESS* and *CHEOPS* but a gap in transitivity means that it could be missed by the *PLATO* mission. Analytically we predict the planet to be right near the edge of transitivity on the secondary star. Numerically, some transits across the secondary star are predicted, however since the secondary star is significantly fainter than the primary such transits unlikely to be observable. The primary transit signature of this system is also a nice illustration that there is generally not a sharp boundary between transits occurring and not. When the planet exits transitivity around 2014 and 2024, it does so “gradually,” mean-

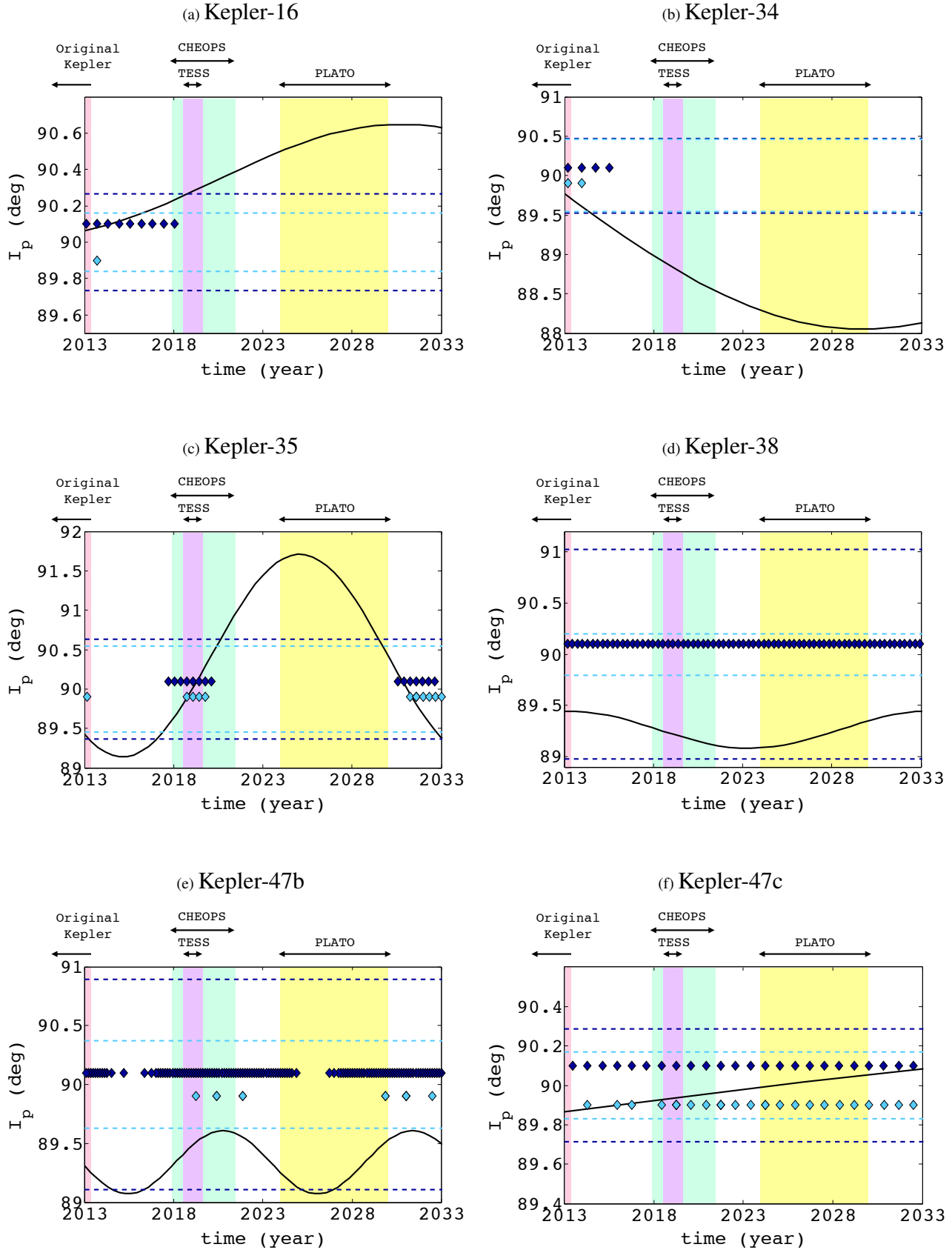


Figure 10. Time evolution of the planet inclination, $I_p(t)$ (black curve) for known transiting circumbinary planets. The limiting inclinations for transitivity (Eq. 34) are shown as horizontal dashed lines for the primary star (dark blue) and secondary star (light blue). Dark and light blue diamonds denote predicted transits on the primary and secondary star, respectively, calculated using an N-body simulation. The vertical position of the diamonds has no physical meaning. Different coloured vertical bands denote the observing windows of different space telescopes, which we label above. Note that the *TESS* timespan commences after the *CHEOPS* timespan because even though *TESS* will launch beforehand, it will only observe the northern hemisphere in its second year.

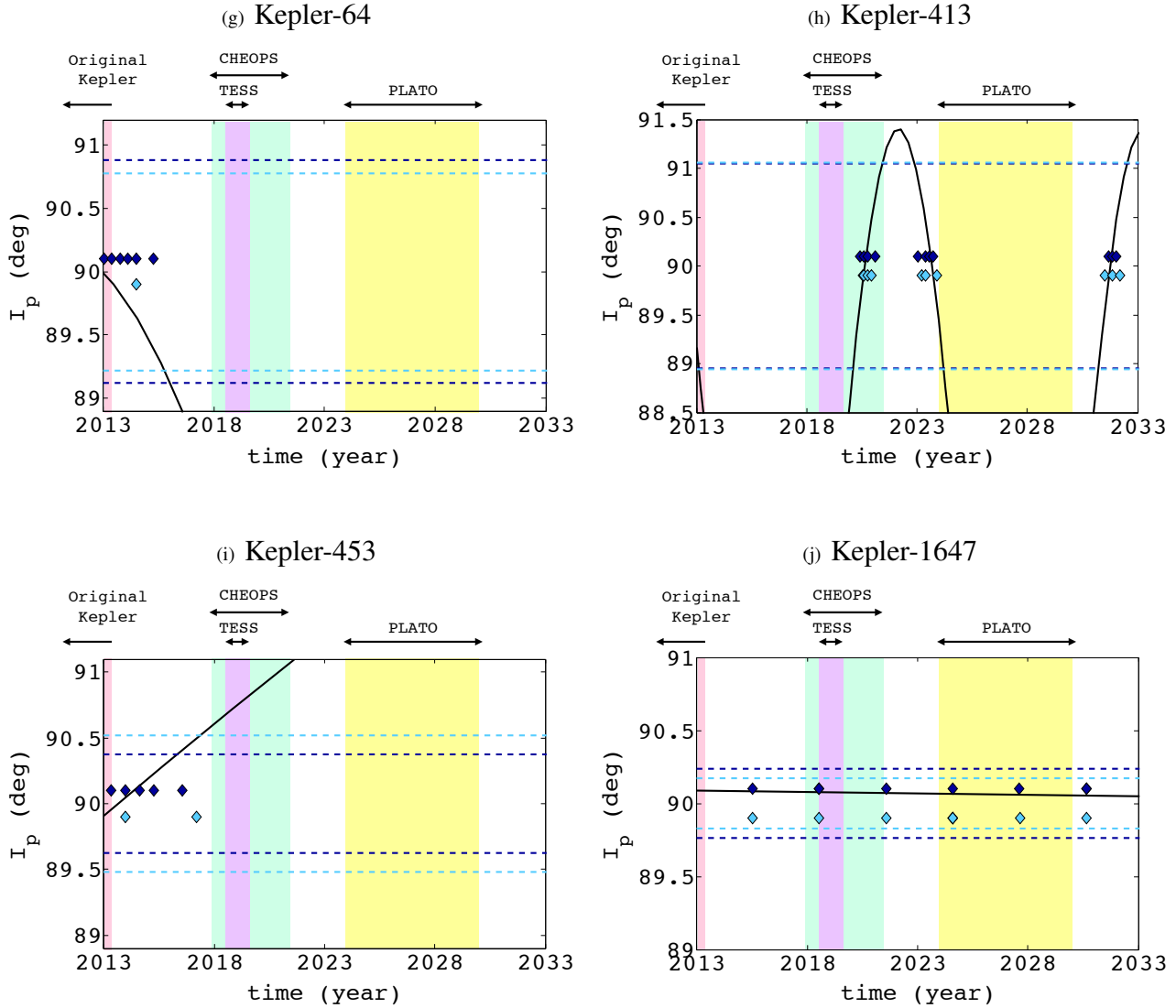


Figure 10. Continued.

Table 2. Observability of the known circumbinary planets discovered so far by *Kepler* and predicted extra similar planets that will later transit. For observability a ✓ indicates analytic predicted transitability and in brackets are the number of transits predicted using N-body simulations

| Name | % primary transitability | % secondary transitability | T_{prec} (yr) | Primary Observability | | | Secondary Observability | | | Predicted extra planets |
|------|--------------------------|----------------------------|------------------------|-----------------------|--------|-------|-------------------------|--------|-------|-------------------------|
| | | | | TESS | CHEOPS | PLATO | TESS | CHEOPS | PLATO | |
| 16 | 42.5 | 30.3 | 41.4 | (0) | ✓(1) | (0) | (0) | (0) | (0) | 0.9 |
| 34 | 16.9 | 16.4 | 69.3 | (0) | (0) | (0) | (0) | (0) | (0) | 3.4 |
| 35 | 36.0 | 30.1 | 19.8 | ✓(3) | ✓(7) | (0) | ✓(3) | ✓(4) | (0) | 0.8 |
| 38 | 100.0 | 0.0 | 20.3 | ✓(3) | ✓(13) | ✓(21) | (0) | (0) | (0) | 0 |
| 47b | 82.5 | 0.0 | 10.6 | ✓(7) | ✓(27) | ✓(30) | (1) | (2) | (1) | 0 |
| 47c | 19.7 | 11.2 | 539.1 | ✓(1) | ✓(4) | ✓(7) | ✓(1) | ✓(4) | ✓(7) | 3.9 |
| 64 | 28.4 | 26.9 | 35.4 | (0) | (0) | (0) | (0) | (0) | (0) | 1.5 |
| 413 | 23.5 | 24.0 | 11.1 | (0) | ✓(4) | (0) | (0) | ✓(3) | (0) | 0.7 |
| 453 | 10.5 | 14.6 | 102.9 | (0) | (0) | (0) | (0) | (0) | (0) | 6.0 |
| 1647 | 7.0 | 5.1 | 7188.7 | (0) | ✓(1) | ✓(2) | (0) | ✓(1) | ✓(2) | 13.2 |

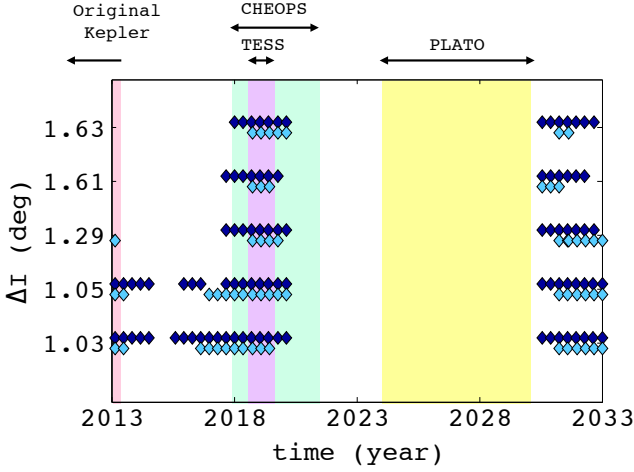


Figure 11. Predicted primary (dark blue diamonds) and secondary (light blue diamonds) for Kepler-35 as a function of the mutual inclination. The five values of ΔI are drawn from the 2σ uncertainty bounds of I_p and Ω_p published in [Welsh et al. \(2012\)](#). From top to bottom, $\Omega_p = -1.57^\circ, -1.57^\circ, -1.24^\circ, -1.0^\circ, -1.0^\circ$ and $I_p = 90.88^\circ, 90.76^\circ, 90.76^\circ, 90.76^\circ$ and 90.67° . Equation 1 is used to calculate ΔI . The middle row of data corresponds to the nominal values in Table. 1.

ing that it goes from transiting every passing to missing a few transits when the orbits are barely overlapping to having transits cease altogether. This is one of the complications that makes a precise analytic derivation of a time-dependent probability difficult.

- **Kepler-47c:** The outermost planet does not have permanent transitivity but transits do not cease until well after the *PLATO* mission. For such a long period planet transitivity is highly efficient, as explained in Sect. 4.3. No predictions are made for the unpublished Kepler-47d, which is believed to reside between planets ‘b’ and ‘c’.

- **Kepler-64/PH-1:** Transits ceased shortly after the end of the *Kepler* mission and will not return for decades.

- **Kepler-413:** The planet with the shortest precession period and largest misalignment generally only produces short bursts of 3-5 transits before an extended absence. It will be observable by *CHEOPS* but unfortunately not *TESS*, and will sneakily transit just before and after the *PLATO*.

- **Kepler-453:** With a similar misalignment to Kepler-413, this planet spends most of its time outside of transitivity. However, with a much larger ratio of T_p/T_{bin} and hence longer T_{prec} , there is no chance of further observations for many decades.

- **Kepler-1647:** One of the longest-period confirmed transiting planet, around one or two star(s), takes over 7,000 years to precess, and hence its orbit is essentially static within the next few decades. Its very long orbital period makes transitivity highly efficiency, but the downside is that its period is similar to the mission lengths, and hence will be missed by *TESS* and only six primary and secondary transits are visible by *CHEOPS* and *PLATO* combined. It also spends very little of its precession period within transitivity.

Finally, is worth noting that the precision of predicted transits decreases the further one looks into the future. This is applicable to planets around both one and two stars; errors in the ephemerides compound and the transit timing uncertainty may become longer than a typical transit duration. For future characterisation say with the *James Webb Space Telescope* or the *European-Extremely Large Telescope*, the astronomical cost and competitiveness of these tele-

scopes makes it impractical to have a very large transit window purely because of “stale” ephemerides.

The problem is amplified for circumbinary planets, owing to the high sensitivity of the transit timings as a function of the orbital parameters. Uncertain ephemerides not only affect the timing of transits but whether or not they occur at all. To illustrate this effect, In Fig. 11 the primary and secondary transit times of Kepler-35 are shown for five different mutual inclinations which are all compatible with the 2σ errors published in [Welsh et al. \(2012\)](#). The middle row of transit times are the same as in Fig. 10c. The number of predicted transits is a sensitive function of ΔI ,⁷ as was discovered in [Martin & Triaud \(2014\)](#) (Fig. 5 in that paper). Better predictions of future transit times requires a re-analysis using the full four years of *Kepler* data (Kepler-35 was published using 671 days of data).

5.2 The number of similar planets await to be found orbiting the same *Kepler* eclipsing binaries

Out of the ten published transiting circumbinary planets, how *lucky* were we to observe them? For a given set of binary and planet parameters, including inclinations, it is interesting to quantify how fortunate we were to have *Kepler*’s four years of observations coincide with the window of transitivity. From this, we can quantify the opposite case of being *unlucky* and missing transits, and hence we can estimate the amount of essentially identical circumbinary planets that may exist around eclipsing binaries discovered by *Kepler*, but have not yet transited.

Define D as the probability of that a continuous observing campaign of length T_{obs} detects a planet transiting that spends $T_{transitivity}$ of its precession period in transitivity,

$$D = \min\left(\frac{T_{obs} + T_{transitivity}}{T_{prec}}, 1\right). \quad (45)$$

For simplicity, simply consider transitivity on the primary star. Equation 45 only works if the planet always transits a couple of times within transitivity, in order to be detectable. For the low mutual inclination *Kepler* planets this is a valid assumption, as demonstrated in Fig. 10. The opposite probability of a failed detection, F , is simply

$$F = \max(1 - D, 1). \quad (46)$$

We can therefore say that for a given system there should be E extra circumbinary systems with essentially identical properties that will transit sometime in the future, and this is calculated as

$$E = \frac{F}{D} \quad (47)$$

$$= \max\left(\frac{T_{prec}}{T_{obs} + T_{transitivity}} - 1, 0\right). \quad (48)$$

Included in Table. 2 is the predicted number of extra planets, where $T_{obs} = 4$ yr. I highlight here a couple of examples. For Kepler-16 $E = 0.9$, which means we are essentially missing another Kepler-16-like planet that will transit in the future. For Kepler-38 $E = 0$ because the planet has permanent transitivity on the primary star and hence cannot evade detection. For Kepler-47b $E = 0$ also, because not only does it spend a large percentage of its time

⁷ Although it seems that *PLATO* has no chance of observing this target.

in transitability but its precision period is only 10.6 yr, the shortest of all known circumbinary planets. At the other extreme, Kepler-453 and -1647 have $E = 6.0$ and 13.2, respectively, owing to long precision periods (particularly for 1647) and short percentages of transitability.

In total these simple estimates predict ~ 30 essentially identical circumbinary planets to ultimately transit *Kepler* eclipsing binaries. The number is reduced to 17 if Kepler-1647 is excluded, for which the wait time may be thousands of years.

6 CONCLUSION

We have derived analytic criteria for the time-dependence of transitability, a state where the planet and binary orbits intersect on the plane of the sky, which is a necessary but not sufficient condition for circumbinary transits. Equations calculated in this paper are applicable to both eclipsing and non-eclipsing binaries and planets of any mutual inclination. This paper improves upon the time-independent criteria derived in [Martin & Triaud \(2015\)](#), and is a key step towards a complete analytic time-dependent transit probability. By calculating future transits of the 10 published transiting circumbinary planets, we predict that 4 may be observable by *TESS*, 7 by *CHEOPS* and 4 by *PLATO*. Interestingly, most of the planets spend less than 50% of their time in transitability, some as low as ~ 10 -20 %. As a consequence, there are likely ~ 17 –30 circumbinary planets around binaries in the eclipsing binary catalog, that have not yet precessed into view. Such new planets may be revealed by the future *TESS* and *PLATO* surveys, or complementary methods such as eclipse timing variations.

7 ACKNOWLEDGEMENTS

A special thank you to Amaury Triaud, with whom I started this project and will ultimately finish it! I have also benefited from constant support by my PhD supervisor Stephane Udry. Thank you to Veselin Kostov who is a dead-set ledge for helping out with some of the orbital elements of the known systems. This work was greatly aided by fruitful conversations with Rosemary Mardling and Javiera Rey. Finally, I thank the anonymous referee for useful suggestions that helped improve the paper, in particular motivating a deeper look into the effects of eccentricity. I also made an extensive use of [ADS](#), [arXiv](#) and the two planets encyclopaediae [exoplanet.eu](#) and [exoplanets.org](#) and thank the teams behind these online tools, which greatly simplify the research.

REFERENCES

Agol, E., Steffen, J., Sari, R., & Clarkson, W. 2005, *MNRAS*, 359, 567
 Armstrong, D. J., Osborn, H., Brown, D., et al., 2014, *MNRAS*, 444, 1873
 Armstrong, D. J., Martin, D. V., Brown, G., et al., 2013, *MNRAS*, 434, 3047
 Barnes, J. W., 2007, *PASP*, 119, 986
 Brakensiek, J. & Ragozzine, D., 2016, *ApJ*, 821, 47
 Borucki, W. J. & Summers, A. L., 1984, *Icarus*, 58, 121
 Chatterjee, S., Ford, E. B., Matsumura, S., & Rasio, F. A. 2008, *ApJ*, 686, 580
 Doolin, S. & Blundell, K. M., 2011, *MNRAS*, 418, 2656

Doyle, L. R., Carter, J. A., Fabrycky, D. C., et al. 2011, *Science*, 333, 1602
 Dvorak, R., 1986, *A&A*, 167, 379
 Dvorak, R., Froeschle, C., & Froeschle, C., 1989, *A&A*, 226, 335
 Farago, F. & Laskar, J., 2010, *MNRAS*, 401, 1189
 Georgakarakos, N. & Eggl, S., 2015, *ApJ*, 802, 2
 Hamers, A. S., Perets, H. B. & Portegies Zwart, S. F., 2016, *MNRAS*, 455, 3180
 Holman, M. J. & Murray, N. W. 2005, *Science*, 307, 1288
 Holman, M. J., & Wiegert, P. A. 1999, *AJ*, 117, 621
 Konacki, M., Muterspaugh, M. W., Kulkarni, S. R. & Helminak, K. G., *A&A*, 704, 513
 Kostov, V. B., McCullough, P. R., Hinse, T. C., et al. 2013, *ApJ*, 770, 52
 Kostov, V. B., McCullough, P. R., Carter, J. A., et al. 2014, *ApJ*, 784, 14
 Kostov, V. B., Orosz, J. A., Welsh, W. F., et al. 2016, *ApJ*, 827, 86
 Hoi Lee, M. & Peale, S. J., 2007, *Icarus*, 190, 103
 Leung, G. C. K. & Hoi Lee, M., 2013, *ApJ*, 763, 107
 Li, G., Holman, M. J., Tao, M., 2016, *arXiv:1608.01768*
 Liu, H.-G., Wang, Y., Zhang, H., Zhou, J.-L., 2014, *A&A*, 790, 141
 Mardling, R. A. & Aarseth, S. J., 2001, *MNRAS*, 321, 398
 Martin, D. V., Mazeh, T. & Fabrycky, D. C., 2015, *MNRAS*, 453, 3354
 Martin, D. V. & Triaud, A. H. M. J., 2014, *A&A*, 570, A91
 Martin, D. V. & Triaud, A. H. M. J., 2015, *MNRAS*, 449, 781
 Martin, D. V. & Triaud, A. H. M. J., 2016, *MNRAS*, 455, L46
 Migaszewski, C. & Goździewski, K., 2011, *MNRAS*, 411, 565
 Muñoz, D. J. & Lai, D., 2015, *PNAS*, 112, 9264
 Orosz, J. A., Welsh, W. F., Carter, J. A., et al. 2012a, *ApJ*, 758, 87
 Orosz, J. A., Welsh, W. F., Carter, J. A., et al. 2012b, *Science*, 337, 1511
 Pilat-Lohinger, E., Funk, B. & Dvorak, R., 2003, 400, 1085
 Rudaux, L., *Sur Les Autres Mondes*, Larousse, 1937, 224 p.
 Sahlmann, J., Triaud, A. H. M. J., Martin, D. V., 2014, *MNRAS*, 447, 287
 Schneider, J. & Chevreton, M., 1990, *A&A*, 232, 251
 Schneider, J. 1994, *Planet. Space Sci.*, 42, 539
 Schwamb, M. E., Orosz, J. A., Carter, J. A., et al. 2013, *ApJ*, 768, 127
 Schwarz, R., Haghighipour, N., Eggl, S., Pilat-Lohinger, E., Funk, B., 2011, *MNRAS*, 414, 2763
 Schwarz, R., Funk, B., Zechner, R., Bazso, A., 2016, *MNRAS*, 460, 3598
 Smullen, R. A., Kratter, K. M., Shannon, A., 2016, *MNRAS*, 461, 1288
 Yates, R. C., *A Handbook on Curves and Their Properties*, Ann Arbor, MI: Edwards, J. W., pp. 155-159, 1952
 Welsh, W. F., Orosz, J. A., Carter, J. A., et al. 2012, *Nature*, 481, 475
 Welsh, W. F., Orosz, J. A., Short, D. R., et al., 2014, *ApJ*, 809, 17